HEAVY-ION SESSION: A (QUICK) INTRODUCTION

B. HIPPOLYTE
Institut Pluridisciplinaire Hubert Curien, Département de Recherches Subatomiques, 23 rue du Loess, F-67037 Strasbourg, France

These proceedings summarise the short introduction given at the beginning of the heavy-ion session of the XLVIII$^{\text{th}}$ Rencontres de Moriond – QCD. The choice is deliberately to focus on global pictures describing the collision of ultra-relativistic heavy ions and its evolution whereas highlights, recent results and latest developments are reported by the other participants of the session. Using mainly Pb–Pb data at the Large Hadron Collider, the emphasis is made on the initial state conditions as well as the observables which qualitatively illustrate how "perfect" and opaque the strongly interacting Quark-Gluon Plasma is.

The basic steps of the evolution of a heavy-ion collision could be described with a single sentence: at first Lorentz contracted ultra-relativistic heavy ions are colliding, leading to a pre-equilibrium phase dominated by initial conditions, very shortly followed by the Quark-Gluon Plasma (QGP) which expands and cools until hadronisation occurs, and eventually long lived particles reach the detectors. Such a short description would certainly not reflect the recent precision measurements presented during the heavy-ion session of this conference. These are performed both at the Large Hadron Collider (LHC) with Pb–Pb collisions at the unprecedented energy of $\sqrt{s_{\rm NN}} = 2.76$ TeV and at the Relativistic Heavy Ion Collider (RHIC) where the gold beam energy is varied (Beam Energy Scan program, BES) corresponding to $\sqrt{s_{\rm NN}} = 7.7$, 11.5, 19.6, 27, 39, 62.4 and 200 GeV with including comparisons to other colliding systems (pp and p–Pb at the LHC; pp, d–Au, Cu–Cu and U–U at RHIC). As an introduction to the session, these proceedings focus on the general picture emerging from several years of study at RHIC and the LHC. The main steps of a heavy-ion collision are presented in section 1 together with some definitions and considerations related to the initial state conditions and the fluctuations observed at that stage. Several global observables and space time properties are discussed in the next section and followed by a qualitative illustration of the QGP opacity.

1 The main steps of the system evolution

Part of the recent progress in the understanding of the evolution of the system created in heavy-ion collisions is illustrated [a] with Fig.1. The initial conditions for the two colliding nuclei are, to a large extent, driven by the geometrical overlap region. The *centrality* of the collision is defined by correlating the multiplicity of the produced particles with the geometry of the system [1]: the most central collisions are the head-on ones for which the multiplicity is the largest. Several quantities are often used to characterise the centrality of the collision: the number of participating nucleons ($N_{\rm part}$), the number of binary collisions ($N_{\rm coll}$, i.e. the number of nucleon-nuclon inelastic collisions) or the geometrical nuclear overlap function ($\mathrm{T_{AA}} = N_{\rm coll}/\sigma^{\rm inel}_{\rm NN}$). Although

[a] it is updated with respect to the one shown at the time of the conference.

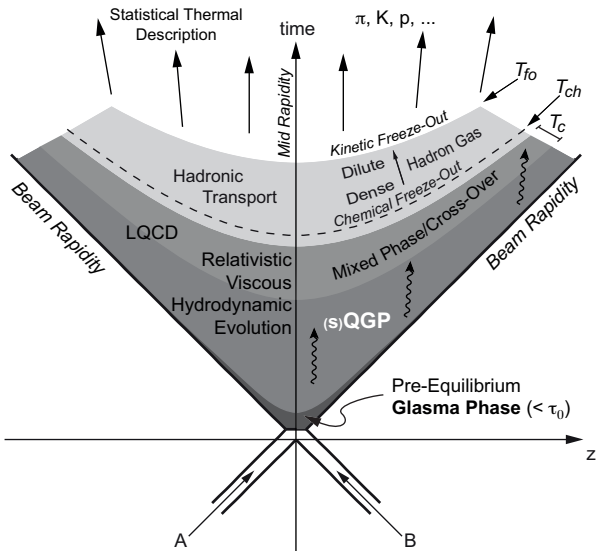

Figure 1: Light cone of the evolution of the system created in heavy-ion collisions at RHIC and the LHC. The main phases and steps are specified on the right side together with the different temperatures driving the transition from the strongly interacting QGP to the hadrons measured in the detectors (successively the critical temperature $T_{\rm c}$ for the chiral symmetry restoration, the chemical freeze-out temperature $T_{\rm ch}$ and the kinetic freeze-out temperature $T_{\rm fo}$). Formalisms used to described successfully this evolution are shown on the left side of the schematisation.

fluctuations in the initial state and their importance were discovered quite recently, they are unambiguously needed for reproducing event-by-event measurements of the anisotropic flow coefficients $v_{n=2,3,4}$ [2] and several contributions of this session are dedicated to that topic [3]. The resulting pre-equilibrium Glasma phase, which includes fluctuations of the energy density distribution on a small scale, is now precisely modelled by combining initial nuclear wave functions and classical Yang-Mills dynamics of the produced color fields [4]. Hard parton scatterings quickly occur, leading to jet and heavy flavour production (see section 3), as well as the thermalisation of the system to the phase where deconfined partons are strongly interacting (sQGP). This fast approach to local thermodynamical equilibrium generally justifies the use of hydrodynamics which is extremely successful for modelling the expansion and the cooling of the QGP (see ref.[5] and references therein).

Lattice QCD (LQCD) calculations provide significant inputs for establishing the equation of state (EOS). The transition between the partonic matter and the hadron gas, as represented in Fig. 1, corresponds to a cross-over and, concerning the value of the (pseudo-) critical temperature for chiral symmetry restoration, there is currently a very good agreement between the Wuppertal-Budapest and HotQCD collaborations: $T_{\rm c} = 155 \pm 3$ (stat.) ± 3 (sys.) MeV [6] and $T_{\rm c} = 154 \pm 8$ (stat.) ± 1 (sys.) MeV [7] respectively. Some systematic uncertainties are still to be resolved for the EOS as can be seen in Fig. 2 (left) which shows the normalised trace anomaly as a function of the critical temperature: the values from both collaborations are compatible below $T_{\rm c}$ but the HotQCD ones are systematically higher by $\sim 25\%$ above $T_{\rm c}$. Later, as it expands and cools, the system consists of a dense then a dilute hadronic gas modelled by hadronic transport codes until particles stop interacting at the kinetic freeze-out. From the statistical analysis of hadron abundances as well as the study of their transverse momentum ($p_{\rm T}$) differential yields, both the chemical freeze-out temperature ($T_{\rm ch}$) and the kinetic freeze-out temperature ($T_{\rm fo}$) can be estimated.

Obviously the presented picture of Fig. 1 remains a simplified one, often used as a guideline to separate "hard" (from the first steps of the collision and involving large momentum transfer between partons) and "soft" probes (corresponding mainly to low $p_{\rm T}$ phenomena) of the QGP. it is important to remember that measures often correspond to observables which are integrated over time and that many questions which are beyond the scope of this introduction stay open,

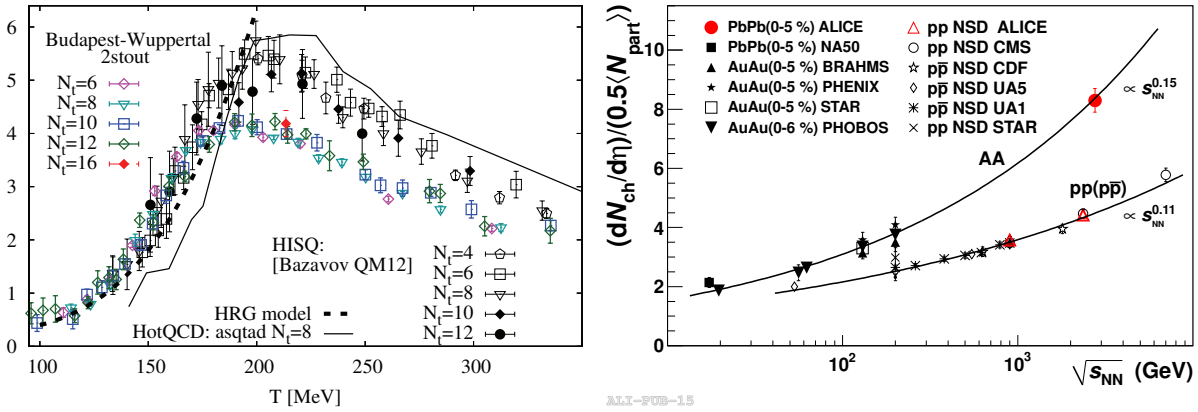

Figure 2: Normalised trace anomaly $(\varepsilon - 3p)/T^4$ as a function of the critical temperature (left): the value of the (pseudo-) critical temperature for chiral symmetry restoration T_c obtained by the Wuppertal-Budapest and HotQCD collaborations is $\simeq 155$ MeV. Number of charged particles produced per unit of pseudorapidity $\mathrm{d}N_{\mathrm{ch}}/\mathrm{d}\eta$ divided by the average number of participant nucleon pairs as a function of the centre of mass energy (right) for both central A-A and non-single diffractive pp (and $\mathrm{p\overline{p}}$) collisions. See text for references.

mainly at the interfaces (e.g. how thermalisation happens so quickly? are other hadronisation mechanisms than fragmentation at play? what are the consequences of such a fast expansion for the system?).

2 Several global observables and space-time properties

The number of charged particles produced per unit of pseudorapidity $\mathrm{d}N_{\mathrm{ch}}/\mathrm{d}\eta$ is among the first measurements performed with heavy-ion collisions at the LHC. ALICE value is shown in Fig. 2 (right) after normalisation by the average number of participant nucleon pairs [8]. Measurements obtained by ATLAS and CMS agree within uncertainties [9,10]. Comparing the value at LHC with lower energy A–A collisions at RHIC and SPS, it can be noted that the evolution of this charged particle multiplicity with $\sqrt{s_{\mathrm{NN}}}$ behaves like a power law and its scaling exponent (0.15) is slightly larger than the one (0.11) extracted from non-single diffractive pp (and $\mathrm{p\overline{p}}$) data. The energy density (ε) for heavy-ion collisions in the central rapidity region can be estimated with the following formula derived from ref. [11]:

$$\varepsilon = \frac{E}{V} = \frac{1}{\pi (r_0 A^{1/3})^2 \, \tau_0} \frac{dE_{\mathrm{T}}}{dy}, \tag{1}$$

where boost invariance is assumed for the energy E (corresponding to the transverse energy per unit of rapidity) and the volume V is defined as the cylinder which radius section is, for central collisions, the one of the colliding nuclei (i.e. $r = r_0 A^{1/3}$ with $r_0 = 1.2$ fm and $A = 208$ for ^{208}Pb) and τ_0 is the formation time. The CMS measurement of the transverse energy per unit of pseudorapidity for the 5% most central collisions gives $\mathrm{d}E_{\mathrm{T}}/\mathrm{d}\eta = 2007 \pm 100$ GeV at mid-rapidity [12]. Choosing a value for τ_0 is a sensible task. Using the conservative value of 1 fm/c, as done at RHIC, leads [b] to an initial energy density of 14 GeV/fm^3 which is almost 3 times the one obtained at RHIC [13] and about a factor 30 above the phase transition expected from LQCD [14].

Basic space-time properties can be inferred from Hanbury Brown–Twiss (HBT) analyses of selected events. The three HBT radii (R_{out}, R_{side} and R_{long}) correspond to the spatial extent along orthogonal directions at decoupling for identified particles [15]. The volume of this homogeneity region ($V \sim (2\pi)^{3/2} R_{\mathrm{out}} R_{\mathrm{side}} R_{\mathrm{long}}$) for charged pions is shown as a function of the

[b] a Jacobian of ~ 1.1 is taken into account; using the charged particle multiplicity, assuming a factor of 3/2 due to the neutral particles and a mean transverse energy per particle of ~ 1 GeV give a similar estimate.

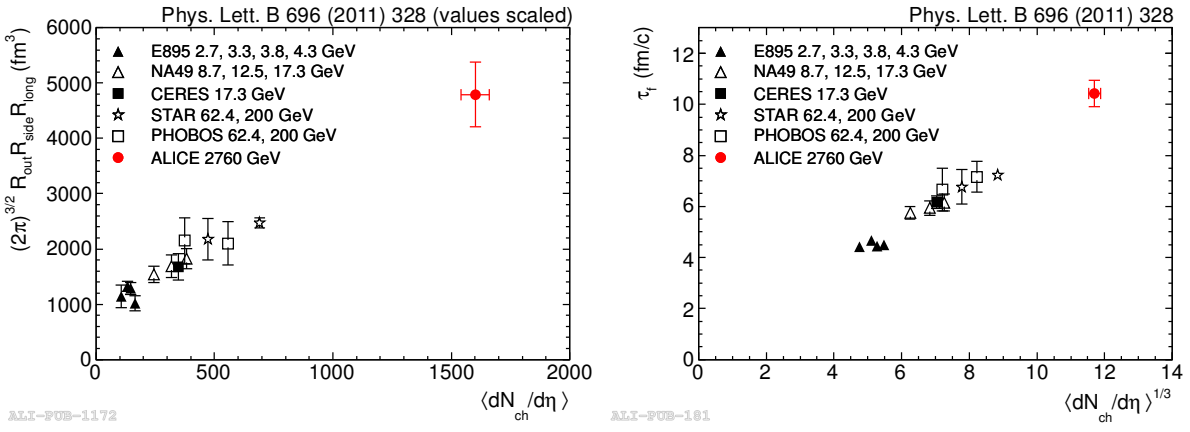

Figure 3: Volume of homogeneity region extracted from the HBT radii $R_{\rm out}$, $R_{\rm side}$ and $R_{\rm long}$ of decoupling pions at $k_\perp = 0.3$ GeV/c as a function of the charged-particle pseudorapidity density (left). Decoupling time extracted from $R_{\rm long}(k_\perp)$ (right). Error bars represent statistical and systematic uncertainties added in quadrature except for E895 where the errors are statistical only. See text for references.

charged particle density in the left panel of Fig. 3 for the most central nucleus–nucleus collisions from AGS to LHC energies [16]. An approximately linear dependence is observed and the volume obtained for Pb–Pb collisions at the LHC is twice as large as the Au–Au one at RHIC while the energy increases from $\sqrt{s_{\rm NN}} = 200$ GeV to 2.76 TeV. The duration of the longitudinal expansion of the system i.e. the decoupling time can be estimated [c] by fitting the $k_\perp$ dependence of $R_{\rm long}$ with fixing $T_{\rm fo}$. In the right panel of Fig. 3, the decoupling time is plotted vs. the cube root of the charged particle density for the most central events: the system lifetime scales linearly and reaches 10 fm/c at the LHC i.e. a value $\sim 30\%$ higher than what was measured at RHIC.

No discussion on anisotropic flow measurements nor comparison with models is given here since the latest results are presented in several other contributions of this session with great details [3]. However, as mentioned in section 1, additional insights on the transverse expansion of the system can be obtained by simply studying hadron integrated yields and low $p_{\rm T}$ spectra. At the LHC energies, the ALICE collaboration reports some tension between the measured protons yields and thermal model predictions from the extrapolation of RHIC energy results [17]: without including the possibility of sudden (non-equilibrium) freeze-out [18], thermal model calculations using $T_{\rm ch} = 164$ MeV would overestimate the proton yields despite being favoured by multi-strange baryon measurements. With respect to the latest implementations of 3D+1 hydrodynamical models followed by hadronic transport, blast-wave fits of hadron $p_{\rm T}$ spectra seem obviously simplistic and outdated. They can still be of interest for systematical studies such as the comparison of the radial flow profile and velocity between RHIC and the LHC energies. For most central events at the LHC, the average transverse flow velocity estimated with the $p_{\rm T}$ spectra of π, K and p is $\langle \beta_{\rm T} \rangle = 0.65 \pm 0.02$ i.e. a 10% increase with respect to similar measurements at RHIC. The value of $T_{\rm fo}$ extracted at the LHC is 95 MeV, similar to the one at RHIC within uncertainties, and decreases with centrality although hydrodynamics does not seem to be fully appropriate for most peripheral events [17].

3 Probing the opacity of the QGP

Characterising some of the properties of the produced matter can be done with "hard probes". The idea is here to use energetic partons produced in the early stages of the collision as a tomographic probe of the system. These partons are expected to interact with the coloured medium and the modification of their evolution can be compared with what would happen in

[c] this is actually an underestimation due to the rapid transverse expansion of the system.

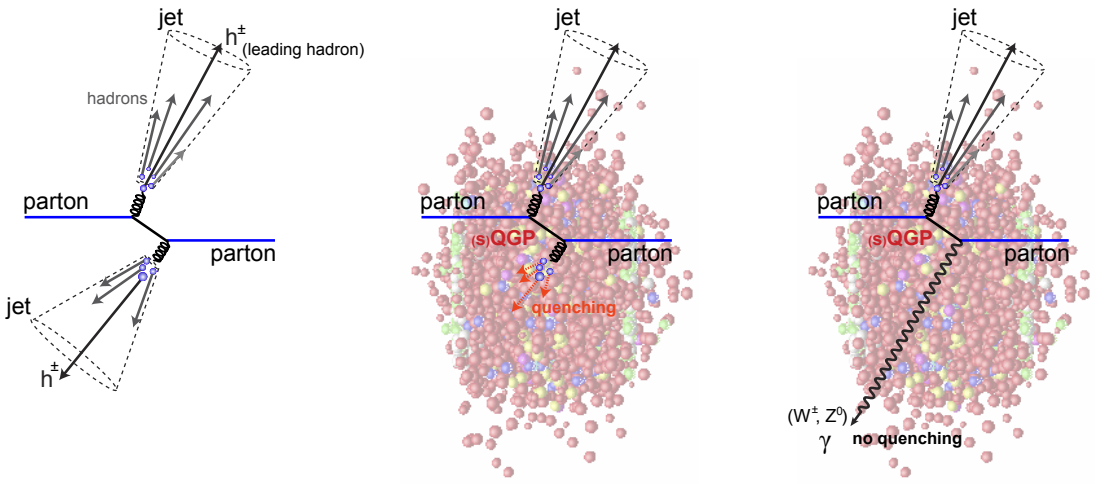

Figure 4: Illustration of jet quenching phenomenon in the presence of a coloured deconfined medium: (left) schematisation of a di-jet event originating from parton scattering in a hadronic collision (no QGP); (centre) when traversing the QGP, one of the scattered parton looses a significant fraction of its energy and the resulting jet, if ever identified and reconstructed, is quenched; (right) when traversing the QGP, photons and electroweak bosons are not affected by the coloured medium and constitute a reference for probing the opacity of the system.

vacuum (or rather for a pp or a p-A collision). For instance, quarkonia can be used to investigate the temperature of the system (for a recent review, see ref.[19]). In this paragraph, only the probes related to the characterisation of the opacity of the system will be mentioned from a qualitative point of view (for a detailed discussion on the corresponding formalism, see ref.[20]). Due to their large mass, heavy-flavoured quarks are produced primarily by gluon fusion at the beginning of the heavy-ion collision. They are supposed to lose energy in the coloured medium very early whereas light-flavoured quarks and gluons lose most of their energy at the end of their propagation. Contrarily, electroweak bosons γ, $W^{\pm}$ and Z^0 are considered as benchmark probes of the QGP because they (as well as their leptonic decays) are not supposed to interact with the hot and dense matter. Figure 4 illustrates the principles of the performed measurements. It is remarkable that a large suppression is seen in almost all hadronic processes when their production rates are compared to pp interactions after normalisation by the number of binary nucleon-nucleon collisions [21,22]. As shown in Fig. 5, for direct photons selected by isolation criteria as well as the $W^{\pm}$ and Z^0 bosons selected via their muonic decay, no deviation from the binary-scaled production is observed. More details on these CMS results can be found in refs.[23]. How these suppressions translate into quantitative measurements of the opacity of the QGP would require much more time than the one allotted for this contribution.

4 Summary

Now that measurements performed in heavy-ion collisions are entering a precision era a clear picture emerges from the main stages of the Quark-Gluon Plasma evolution. Many results are already available at the LHC but also at RHIC with the Beam Energy Scan which turns on/off key features and it is currently a question of testing thoroughly the validity of models/descriptions from 7.7 GeV to 2.76 TeV. With the upgrades of the experiments after the Long Shutdown 1 and 2, additional statistics will allow for further differential measurements.

Acknowledgments

The author wish to thank the organisers for the pleasant and inspiring atmosphere during the conference.

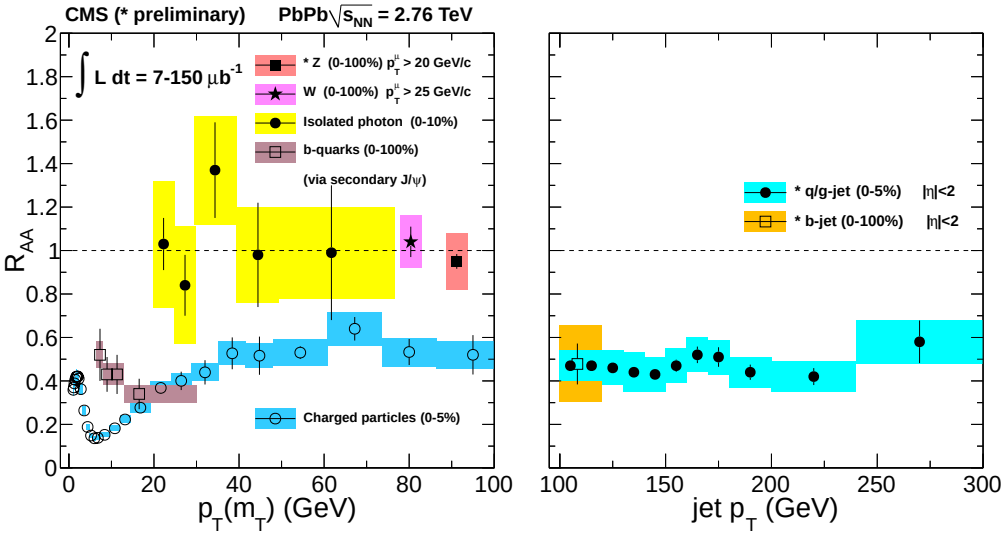

Figure 5: Nuclear modification factor as a function of transverse momentum p_{T} or transverse mass m_{T}. No suppression is observed for isolated photons, W and Z bosons contrarily to charged particles and b-quarks (identified using non-prompt J/ψ) (left). A similar suppression ($\mathrm{R_{AA}} \sim 0.5$) is seen for quark- and gluon-jets as well as for b-jets at high p_{T} (right). Centrality selections vary depending on the considered particles. See text for references.

References

1. B. Abelev *et al* (ALICE Collaboration), arXiv:1301.4361.
2. B. Schenke *et al*, *Nucl. Phys.* B **904–905**, 409c (2013).
3. Y. Pandit *et al* (STAR Collaboration), these proceedings; Q. Wang *et al* (CMS Collaboration), these proceedings; A. Andreazza *et al* (ATLAS Collaboration), these proceedings.
4. B. Schenke, P. Tribedy and R. Venugopalan, *Phys. Rev. Lett.* **108**, 252301 (2012). and C. Gale *et al*, *Phys. Rev. Lett.* **110**, 012302 (2013).
5. M. Luzum, *J. Phys.* G **38**, 124026 (2011).
6. S. Borsanyi *et al* (Wuppertal-Budapest Collaboration), JHEP 1009, 073 (2010).
7. A. Bazavov *et al* (HotQCD Collaboration), *Phys. Rev.* D **85**, 054503 (2012).
8. K. Aamodt *et al* (ALICE Collaboration), *Phys. Rev. Lett.* **105**, 252301 (2010)
9. G. Aad *et al* (ATLAS Collaboration), *Phys. Lett.* B **710**, 363 (2012).
10. S. Chatrchyan *et al* (CMS Collaboration), *JHEP* **1108**, 141 (2011).
11. J.D. Bjorken *Phys. Rev.* D **27**, 140 (1983).
12. S. Chatrchyan *et al* (CMS Collaboration), *Phys. Rev. Lett.* **109**, 152303 (2012).
13. S.S Adler *et al* (PHENIX Collaboration), *Phys. Rev.* C **71**, 034908 (2005).
14. S. Borsanyi *et al* (Wuppertal-Budapest Collaboration), JHEP 1011, 073 (2010).
15. M.A. Lisa *et al Ann. Rev. Nucl. Part. Sci* **55**, 357 (2005).
16. K. Aamodt *et al* (ALICE Collaboration), *Phys. Lett.* B **696**, 328 (2011).
17. B. Abelev *et al* (ALICE Collaboration), *Phys. Rev. Lett.* **109**, 252301 (2012) and arXiv:1303.0737.
18. M. Petran, J. Letessier, V. Petracek and J. Rafelski, arXiv:1303.2098.
19. A. Mocsy, P. Petreczky and M. Strickland, *Int. J. Mod. Phys.* A **28**, 1340012 (2013).
20. N. Armesto *et al Phys. Rev.* C **86**, 064904 (2011).
21. B. Abelev *et al* (ALICE Collaboration), *Phys. Lett.* B **720**, 52 (2013).
22. S. Chatrchyan *et al* (CMS Collaboration), *Eur. Phys. J* C **72**, 1945 (2012).
23. Y. Mao *et al* (CMS Collaboration), these proceedings; G. Roland *et al* (CMS Collaboration), *Nucl. Phys.* B **904–905**, 43c (2013); C. Mironov *et al* (CMS Collaboration), *Nucl. Phys.* B **904–905**, 194c (2013).